NAVAL POSTGRADUATE SCHOOL

Monterey, California

NUMERICAL SIMULATION OF

STEADY-STATE FRONTS

by

R. T. Williams

August 1973

NAVAL POSTGRADUATE SCHOOL

Monterey, California

Rear Admiral M. B. Freeman
Superintendent

M. U. Clauser
Provost

ABSTRACT:

The numerical frontogenesis model of Williams (1972) is modified to include horizontal and vertical turbulent diffusions of heat and momentum. The turbulent diffusions are represented with constant coefficients, and an Ekman layer is added to the basic deformation field. The numerical solutions show realistic quasi-steady fronts forming within 1 - 2 days. These solutions are examined and compared over a wide range of the various coefficients.

This task was supported by: The Environmental Prediction Research Facility and the Foundation Research Program at the Naval Postgraduate School which is funded by the Chief of Naval Research.

NPS-51Wu73081A
August 1973

TABLE OF CONTENTS

1. Introduction

Hoskins and Bretherton (1972) have shown analytically, and Williams (1967, 1972) has shown numerically that discontinuous fronts can form within a finite period of time if no turbulent diffusion is present. These studies suggest that a discontinuity will form within 24 to 36 hours when reasonable initial conditions are used. If turbulent diffusion is present, it can be expected that a balance will be achieved between the frontogenetic advections and the turbulent diffusions of heat and momentum. The front should remain in this state of quasi-balance as long as the large scale deformation field causes frontogenetic advections around the front. The purpose of this study is to obtain and examine steady-state frontal solutions. Welander (1963) obtained steady-state frontal solutions with a boundary layer technique, but his formulation did not involve a frontogenetic large-scale deformation field.

The turbulent diffusion coefficients for heat and momentum are taken to be constant in this study, although these coefficients are actually functions of the wind and temperature fields. Smagorinsky (1963) and Leith (1968) have proposed forms for the horizontal diffusion coefficients which are dependent on the local wind field. Many studies have treated the form of the vertical diffusion coefficients near the surface (Estoque 1960, Deardorff 1970, 1972). In this study we will carry out a large number of integrations with different values of the various constant coefficients. The range of values will include the mean values which are given by the various nonlinear formulations.

This investigation will employ the numerical model of Williams (1972); this reference will hereafter be referred to as W72. The physical model is essentially the same as one of the models treated by Hoskins (1971) and Hoskins and Bretherton (1972). The frontogenesis is forced by a non-divergent horizontal wind field which contains stretching deformation. The hydrostatic primitive equations are used with the Boussinesq approximation. In the model the time dependent quantities are functions of y and z only.

The basic deformation wind field is constant in time and is independent of height, except in the surface boundary layer.

In Section 2, the basic forecast equations are developed, and a simplification which keeps the problem two-dimensional is discussed. The initial conditions are presented in Section 3. The solutions which contain only horizontal diffusion are discussed in Section 4, and those which contain only vertical diffusion are discussed in Section 5. The combined experiments which include both types of diffusion are examined in Section 6 and the conclusions are given in Section 7.

2. Basic equations

The hydrostatic Boussinesq equation with diffusion may be written:

$$\frac{\partial}{\partial t}\underset{\sim}{V} + \nabla \cdot (\underset{\sim}{V}\underset{\sim}{V}) + \frac{\partial}{\partial z}(w\underset{\sim}{V}) + \nabla\phi + f\underset{\sim}{k} \times \underset{\sim}{V} = A\nabla^2 \underset{\sim}{V} + C_m \frac{\partial^2 \underset{\sim}{V}}{\partial z^2}, \qquad (2.1)$$

$$\frac{\partial \theta}{\partial t} + \nabla \cdot (\theta \underset{\sim}{V}) + \frac{\partial}{\partial z}(w\theta) = A\nabla^2\theta + C_\theta \frac{\partial^2 \theta}{\partial z^2} + Q_a, \qquad (2.2)$$

$$\nabla \cdot \underset{\sim}{V} + \frac{\partial w}{\partial z} = 0, \qquad (2.3)$$

$$\frac{\partial \phi}{\partial z} = \frac{g\theta}{\theta_o}, \qquad (2.4)$$

where the notation is the same as used in W72. The quantity A is the horizontal turbulent diffusion coefficient; note that the same value is used for both heat and momentum. The quantities C_m and C_θ are the vertical turbulent diffusion coefficients for momentum and heat respectively. A convective adjustment process is represented by the function Q_a. The boundary conditions at the top and bottom of the domain are:

$$\left.\begin{aligned} & w(x,y,o,t) = w(x,y,H,t) = 0 \\ & \underset{\sim}{V}(x,y,o,t) = 0 \\ & C_m \frac{\partial \underset{\sim}{V}}{\partial z}(x,y,H,t) = 0 \\ & C_\theta \frac{\partial \theta}{\partial z}(x,y,o,t) = C_\theta \frac{\partial \theta}{\partial z}(x,y,H,t) = 0 \end{aligned}\right\} . \qquad (2.5)$$

The lower boundary conditions are realistic for fronts over land, but the upper lid boundary conditions give only a rough approximation to the tropopause. Upper frontogenesis has been treated by Hoskins and Bretherton (1972) and Hoskins (1972). In this paper our main concern is with fronts in the lower troposphere.

The following fields which satisfy the boundary conditions (2.5) are approximate solutions to the steady-state equations [(2.1) - (2.4)] :

$$\left.\begin{aligned} \underset{\sim}{V} = \underset{\sim}{U} &\equiv D\left\{[x(1 - e^{-Bz}\cos Bz) + ye^{-Bz}\sin Bz]\underset{\sim}{i}\right. \\ &\left.-[y(1 - e^{-Bz}\cos Bz) - xe^{-Bz}\sin Bz]\underset{\sim}{j}\right\} \\ w &= 0 \\ \phi = \Phi &\equiv -D^2(x^2 + y^2)/2 - fDxy \\ \theta &= 0 \end{aligned}\right\}, \qquad (2.6)$$

where $B = (f/2C_m)^{1/2}$ and where D and f are constant. These relations satisfy the steady-state equations if some small advection terms in the boundary layer are neglected. These small terms are usually dropped in the Ekman theory and they are of the order of the Rossby Number which for these fields is D/f. In this paper D/f = 0.1 for all cases.

We now subdivide our dependent variables as follows:

$$\left.\begin{aligned} \underset{\sim}{V} &= \underset{\sim}{U}(x,y,z) + u(y, z, t)\underset{\sim}{i} + v(y,z,t)\underset{\sim}{j} \\ w &= w(y, z, t) \\ \theta &= \theta(y, z, t) \\ \phi &= \Phi(x,y) + \pi(y, z, t) \end{aligned}\right\}, \qquad (2.7)$$

It is noted that all departures from the steady deformation solutions (2.6) are assumed to be independent of x. If we substitute the relations (2.7) in the $\underset{\sim}{i}$ component of (2.1) we obtain:

$$\begin{aligned} &\frac{\partial u}{\partial t} + \frac{\partial}{\partial y}(uv) + \frac{\partial}{\partial z}(wu) + uD(1 - e^{-Bz}\cos Bz) \\ &-D[y(1 - e^{-Bz}\cos Bz) - xe^{-Bz}\sin Bz]\frac{\partial u}{\partial y} + vDe^{-Bz}\sin Bz \\ &+wD\frac{\partial}{\partial z}\left[xe^{-Bz}(1 - \cos Bz) + ye^{-Bz}\sin Bz\right] = fv + A\frac{\partial^2 u}{\partial y^2} + Cm\frac{\partial^2 u}{\partial z^2}. \end{aligned} \qquad (2.8)$$

Please note that the assumption that u is independent of x for all time is violated in (2.8) in the two terms where x appears. This indicates that the other quantities which were assumed independent of x are, in fact,

x-dependent and this would bring other terms into the equations. In this study we will neglect these added terms and apply (2.8) and the other equations at x = 0. If the initial u, v, w, θ, and π fields are independent of x the error from this approximation will grow slowly and it will be confined to the boundary layer since the x-dependent terms in (2.8) are zero outside the boundary layer. Since frontogenesis occurs very rapidly, it is expected that the development of x-variations in the dependent variables would have only a small effect on the resulting quasi-steady front. In any case these effects could not be observed in the atmosphere, because atmospheric fronts always have some variation in the basic fields along the front which would be much more important.

When Eq. (2.8) is evaluated at x = 0 it becomes:

$$\frac{\partial u}{\partial t} + \frac{\partial (uv)}{\partial y} + \frac{\partial (wu)}{\partial z} - \Gamma u \frac{\partial V}{\partial y} + \Gamma V \frac{\partial u}{\partial y} - v \frac{\partial V}{\partial y} e^{-Bz} \sin Bz$$

$$-Vw \frac{\partial}{\partial z}(e^{-Bz} \sin Bz) = fv + A\frac{\partial^2 u}{\partial y^2} + C_m \frac{\partial^2 u}{\partial z^2} \quad , \tag{2.9}$$

where: $V = -Dy$ and $\Gamma = 1 - e^{-Bz}\cos Bz$. The $\underset{\sim}{j}$ component of (2.1) applied at x = 0 takes the form:

$$\frac{\partial v}{\partial t} + \frac{\partial}{\partial y}(vv) + \frac{\partial}{\partial z}(wv) + \Gamma \frac{\partial}{\partial y}(vV) - u \frac{\partial V}{\partial y} e^{-Bz} \sin Bz$$

$$-wV \frac{\partial}{\partial z}(e^{-Bz} \cos Bz) = -\frac{\partial \pi}{\partial y} - fu + A\frac{\partial^2 v}{\partial y^2} + C_m \frac{\partial^2 v}{\partial z^2} \quad . \tag{2.10}$$

In a similar manner Eq. (2.2) may be written:

$$\frac{\partial \theta}{\partial t} + \frac{\partial (v\theta)}{\partial y} + \frac{\partial}{\partial z}(w\theta) + \Gamma V \frac{\partial \theta}{\partial y} = A\frac{\partial^2 \theta}{\partial y^2} + C_\theta \frac{\partial^2 \theta}{\partial z^2} + Q_a \quad , \tag{2.11}$$

and Eqs. (2.3) and (2.4) become:

$$\frac{\partial v}{\partial y} + \frac{\partial w}{\partial z} = 0 \quad , \tag{2.12}$$

$$\frac{\partial \pi}{\partial z} = \frac{g\theta}{\theta_0} \quad . \tag{2.13}$$

The boundary conditions at the top and the bottom of the domain are given by:

$$u = v = w = C_\theta \frac{\partial \theta}{\partial z} = 0, \quad z = 0$$
$$C_m \frac{\partial u}{\partial z} = C_m \frac{\partial v}{\partial z} = w = C_\theta \frac{\partial \theta}{\partial z} = 0, \quad z = H \qquad (2.14)$$

where H is the distance between the rigid plates. The no slip condition at the lower boundary and the no strex condition at the top roughly represent the troposphere.

If we define the vertical average of a quantity as

$$\langle (\ ) \rangle \equiv \frac{1}{H} \int_0^H (\ ) dz,$$

and integrate the hydrostatic equation (2.13) with respect to z and remove the vertical mean, we obtain

$$\pi - \langle \pi \rangle = \frac{g}{\theta_o} \left[\int_0^z \theta dz - \left\langle \int_0^z \theta dz \right\rangle \right]. \qquad (2.15)$$

Take the vertical average of (2.12) and use the boundary conditions (2.14), which gives

$$\frac{\partial}{\partial y} \langle v \rangle = 0.$$

This equation states that the total mass flux in the $\underset{\sim}{j}$ direction is independent of y. In W72 a symmetry argument was used to show that this flux must be zero. This argument does not hold strictly in our case, but it can be expected that at large distances from the frontal zone the disturbance mass flux will vanish.

Thus we set

$$\langle v \rangle = 0. \qquad (2.16)$$

If we utilize the development in W72 we can rewrite (2.10) in the following form:

$$\frac{\partial v}{\partial t} + \frac{\partial}{\partial y}\left[vv - \langle vv\rangle\right] + \frac{\partial (wv)}{\partial z} + \frac{\partial}{\partial y}\left(\Gamma vV - \langle \Gamma v\rangle V\right)$$

$$- \frac{\partial V}{\partial y}\left[ue^{-Bz}\sin Bz - \langle ue^{-Bz}\sin Bz\rangle\right] - V\left\{w\frac{\partial}{\partial z}(e^{-Bz}\cos Bz)\right.$$

$$\left. - \left\langle w\frac{\partial}{\partial z}(e^{-Bz}\cos Bz)\right\rangle\right\} = -\frac{\partial}{\partial y}(\pi - \langle\pi\rangle) - f(u - \langle u\rangle)$$

$$+ A\frac{\partial^2 v}{\partial y^2} + C_m\left[\frac{\partial^2 v}{\partial z^2} + \frac{1}{H}\left(\frac{\partial v}{\partial z}\right)_{z=0}\right]. \qquad (2.17)$$

The Eqs. (2.9), (2.11), (2.12), (2.15), and (2.17) form a complete set which can be solved by a pure marching process. The finite difference equations conserve mean squares in the advection terms and are described by Williams (1967). The frictional terms are evaluated at the previous time step to avoid computational instability. Computational boundaries are introduced at $y = \pm Y$ and these are the same as used in W72. On these boundaries u and θ are held fixed and $v = 0$.

3. Initial conditions

The initial conditions are the same as those employed in W72. The initial temperature field is given by

$$\theta(y, z, o) = \frac{\partial \bar{\theta}_I}{\partial z}(z - H/2) - a(2/\pi)\arctan(\sinh \alpha y), \qquad (3.1)$$

where $\alpha = f\,\pi\, H^{-1}(g\theta_o^{-1}\ \partial\bar{\theta}_I/\partial z)^{-1/2}$. The quantity $\partial\bar{\theta}_I/\partial z$, which is constant, is the initial static stability and a is one half the total horizontal temperature variation

The initial x - component of the velocity is given by

$$u(y, z, o) = \frac{2}{\pi}\frac{ga\alpha}{f\theta_o}(z - H/2)\,\mathrm{sech}\,\alpha y. \qquad (3.2)$$

This equation is obtained by substituting (3.1) into the thermal wind equation and integrating. In this study the v field is the divergent part part of the wind. We initialize the v field by equating it to the divergent part of the wind which is obtained from the quasi-geostrophic equations.

The details are given in W72.

It is noted that these initial conditions do not satisfy the boundary conditions on u, v, and θ at the upper and lower boundaries. A period of adjustment will be required to form the surface friction layer and some oscillations may be observed later.

4. Numerical experiments with horizontal diffusion

All numerical results to be shown use the following values for the constants:

$$\left.\begin{aligned} &f = 10^{-4}\ \text{sec}^{-1}\ , \quad \frac{g}{\theta_o} = .0327\ \text{m sec}^{-2}(^oK)^{-1} \\ &H = 9\ \text{km}, \quad Y = 1800\ \text{km} \\ &D = 10^{-5}\ \text{sec}^{-1}\ , \quad \partial\bar{\theta}_I/\partial z = 4^oK\ \text{km}^{-1} \\ &a = 12.56K \end{aligned}\right\} . \tag{4.1}$$

These values were also used in W72.

In this section we examine the numerical solutions which include only horizontal diffusion, so that $C_m = C_\theta = 0$. Many numerical experiments are examined in this section which have values of the horizontal diffusion coefficient ranging from $A = 10^{+3}\ m^2sec^{-1}$ to $A = 10^6 m^2sec^{-1}$. All experiments in this section have a vertical increment of $\Delta z = 333$ m. The horizontal mesh length is either 20 km or 60 km depending on the expected frontal scale. The convective adjustment process Q_a is not required in these experiments.

A reasonable measure of the width of the frontal zone is given by

$$d \equiv \frac{\theta(-Y,\ z,\ o) - \theta(Y,\ z,\ o)}{\left|\partial\theta/\partial y\right|_{max}} , \tag{4.2}$$

where $\partial\theta/\partial y$ is approximated by a one-sided difference. Figure 1 shows the variation of d for 3 different experiments at the lowest level (z = 167 m). The lowest curve which is taken from W72 is for the frictionless case (A = 0) with $\Delta y = 20$ km. In this experiment no steady-state is reached

although d is bounded by Δy because of the truncation error. In W72 it was estimated that a discontinuity would occur at t = 1.75 days if there were no numerical truncation error. The middle curve corresponds to the experiment with A = 3 x $10^4 m^2 sec^{-1}$ and Δy = 20 km, and shows that the solution reaches a steady-state at 2 days and is close to the limiting scale within 1.5 days. The upper curve is for A = 5 x 10^5 $m^2 sec^{-1}$ and Δy = 60 km. This experiment shows the same behavior as with the smaller diffusion coefficient except that the limiting scale is much larger.

Figure 2 contains cross sections of $\theta' = \theta - \overline{\theta}_I$, where θ is the horizontally averaged initial potential temperature. Only the lower half plane is shown because the solutions of this section satisfy the symmetry condition which is given by Eq. (5.4) in W72. Also, the outer portion of the domain between $|y|$ = 1200 km and $|y|$ = 1800 km is not shown. The solutions shown in the remainder of this section are for t = 4 days. The solutions in Fig. 2 may be compared with the initial conditions and the frictional solutions which are shown in Figure 4 of W72. The solution for A = 3 x $10^4 m^2 sec^{-1}$ is very similar to the frictionless solution at t = 1.25 days except that the frictional case has a larger tilt. The solution for A = 5 x $10^5 m^2 sec^{-1}$ is similar to the solution for A = 3 x $10^4 m^2$ sec^{-1} except that the gradients are much weaker and the frontal zone has slightly less tilt.

Figure 3 contains cross sections of u for the same cases and these can be compared with Figure 5 in W72. As noted above, the solution for A = 3 x $10^4 m^2 sec^{-1}$ is very similar to the frictionless solution at t = 1.25 days, except that the tilt is greater for the frictional case. The solution for A = 5 x $10^5 m^2 sec^{-1}$ is similar to the solution A = 3 x $10^4 m^2 sec^{-1}$ except that the velocities are much smaller and the gradients are much weaker.

Figure 4 summarizes all the numerical experiments which contain only horizontal diffusion. The figure contains the frontal scale at z = 167 m as a function of the diffusion coefficient on a log-log plot. The dots represent experiments with Δy = 60 km and the circles represent experiments with Δy = 20km. For comparison, let us derive the quasi-geostrophic solution at z = 0. The steady-state first law of thermodynamics

at the surface is

$$-Dy\frac{\partial\theta'}{\partial y} = A\frac{\partial^2\theta'}{\partial y^2} \quad . \tag{4.3}$$

The solution to this equation is

$$\theta'(y, o) = \left(\theta'(\infty,o) - \theta'(-\infty,o)\right)(2A\pi/D)^{1/2}\int_o^y \exp\left(-\frac{Dy^2}{2A}\right) dy \quad . \tag{4.4}$$

When this form is substituted into the definition we obtain

$$d = (2A\pi/D)^{1/2} \quad , \tag{4.5}$$

which is shown in Figure 4. The plotted data approach the line (4.5) as A becomes large, which is expected because the larger scales involved should lead to more nearly quasi-geostrophic solutions (Williams, 1967). As A is decreased the points fall farther below the curve although the slope is not much greater than $\frac{1}{2}$. This is the effect of the advections of temperature and momentum by the divergent part of the wind. These effects are neglected in the quasi-geostrophic equations. For the smallest values of A the plotted data again approach and cross the quasi-geostrophic curve. This is a consequence of the truncation error which arises when the scale becomes very small.

5. Numerical experiments with vertical diffusion

In this section we examine the numerical solutions which include only the vertical diffusion so that A = 0. Both vertical diffusion coefficients are varied over a range from 1.25 m^2sec^{-1} to 15 m^2sec^{-1}. The grid increments for all of these experiments are Δy = 60km and Δz = 200m. This value of the vertical increment was chosen to resolve better the vertical structure of the frontal zone and the surface friction layer. In these experiments the convective adjustment process Q_a is required at times near the surface on the cold air side of the front.

In most of the experiments C_m and C_θ are not equal because they are normally different in the lower troposphere due to the influence of thermal

stratification. Figure 5 shows the variation of the frontal scale for 3 combinations of C_m and C_θ. These curves may be compared with Figure 1 which gives solutions with horizontal diffusion only. The solutions in Figure 5 all show oscillations which were not present in the horizontal diffusion cases. These oscillations arise from the development of the surface boundary layer which is not present in the initial conditions. The interior fields must adjust to the no-slip velocity condition and to the insulated potential temperature condition at the lower boundary. The delay in frontogenesis in the first few hours between Figures 5 and 1 is also due to the adjustment process. At t = 4 days the upper 2 curves in Figure 5 are nearly steady while the lowest curve ($C_m = 10 m^2 sec^{-1}$, $C_\theta = 1.25 m^2 sec^{-1}$) still contains oscillations. We will compare the various solutions in this section at t = 4 days although those experiments which have a small C_θ may not be quite steady.

Figure 6 contains cross sections of θ' for the 3 experiments at t = 4 days. The solutions in this section do not have the vertical symmetry properties which were noted in the previous section because the upper and lower boundary conditions are not equal. Nevertheless we display only the solutions for the lower half of the domain because we are concerned mainly with fronts near the surface and also because the solutions near the upper boundary are not very realistic. The solutions in Figure 6 may be compared with the horizontal diffusion solutions which are given in Figure 2. Comparison of these figures shows some important differences between steady-state fronts in which only vertical diffusion is present. The fronts with vertical diffusion all show a greater tilt than those with only horizontal diffusion. The solution with the smallest vertical heat diffusion coefficient ($C_m = 10\ m^2 sec^{-1}$, $C_\theta = 1.25\ m^2 sec^{-1}$) has a large tilt in the lower 2 kilometers of the atmosphere. The vertical diffusion in these experiments causes the large gradient region to extend higher into the atmosphere than for those experiments with only horizontal diffusion. It is noted that $\partial\theta'/\partial z$ is negative near the lower boundary, and this comes from the insulated boundary condition at z = 0:

$$\frac{\partial \theta}{\partial z} = 0 = \frac{\partial \bar{\theta}_I}{\partial z} + \frac{\partial \theta'}{\partial z} , \tag{5.1}$$

since $\partial\bar{\theta}_I/\partial z$ is positive.

Figure 7 contains cross sections of the u field for the 3 experiments at t = 4 days. These solutions can be compared with the horizontal diffusion solutions which are shown in Figure 3. All of the solutions show the presence of the surface friction layer with the no-slip boundary condition. The thickness of the surface boundary layer appears to vary in proportion to $C_m^{1/2}$ as would be predicted by Ekman theory. When these fields are compared with the temperature fields in Figure 6, it can be seen that the regions of large cyclonic shear and large vertical shear occur in the zones of large temperature gradient. As would be expected, the maximum speed occurs in the experiment with the minimum value of the momentum diffusion coefficient (C_m = 1.25 $m^2 sec^{-1}$, C_θ = 5 $m^2 sec^{-1}$).

Figure 8 summarizes all the numerical experiments which contain only vertical diffusion. The data for each experiment at t = 4 days and z = 100 m are plotted as a function of C_m and C_θ. The number above each point is the frontal scale d and the number below each point is the frontal location y_f. A striking feature of the diagram is the tendency for d to remain relatively constant as C_m is increased when C_θ is held fixed. Conversely d increases rapidly with C_θ when C_m is held fixed. The quantity y_f is a measure of the mean frontal tilt because in the center of the domain (z = 4.5 km) the frontal zone is located near y = 0 (see Figures 2 and 6). As noted above some experiments have a much larger tilt in the lower 2 kilometers. Figure 8 shows a slow increase in the tilt as C_m is increased for a fixed C_θ. When C_m is held fixed the tilt decreases more rapidly as C_θ is increased. The experiments for the special cases C_m = 0 and C_θ = 0 are not included in the figure. The experiment for C_m = 10 $m^2 sec^{-1}$ and C_θ = 0 contains large special oscillations while the solution for C_m = 0 and C_θ = 5 $m^2 sec^{-1}$ contains large time fluctuations.

Some of the gross features of Figure 8 may be interpreted as follows. Consider the behavior for fixed C_θ. As C_m is increased we expect the vertical wind to decrease and through the thermal wind equation this should decrease the horizontal temperature gradient. There is, however, an opposing effect in the surface boundary layer. In the region of cyclonic vorticity we expect horizontal mass convergence in the boundary layer;

this should occur even if the boundary layer is not of the pure Ekman type (Mak, 1972). This convergence will tend to build up the temperature gradients within the friction layer. This effect is opposed in part by the vertical diffusion of heat which is proportioned to C_θ. As C_m is increased the boundary layer will become thicker, as was pointed out earlier in this section. This increase in the thickness of the friction layer will tend to increase the temperature gradients as long as C_θ is held fixed. The numerical solutions show that this frictional convergence effect on the temperature gradient is approximately balanced by the momentum diffusion effect through the thermal wind. Therefore d remains nearly constant as C_m is increased with C_θ held fixed.

When C_m is held fixed and C_θ is decreased the vertical scale of the frontal zone becomes very small. This can be seen in Figure 6 if the lower 2 cross sections are compared. The horizontal temperature gradient is somewhat constrained through the thermal wind relation by vertical momentum diffusions. The decrease in the vertical scale, which comes from a decrease in C_θ, must be associated with an increase in the tilt of the frontal zone if the change in the horizontal gradient is to be minimized. This behavior is clearly present in Figure 8.

6. Numerical experiments with both horizontal and vertical diffusion

In this section we will examine the solutions which contain both horizontal and vertical diffusion. Individual solutions will not be shown because they are essentially combinations of the solutions shown in earlier sections. The principal features of the solutions are summarized in Tables 1 and 2. All solutions have space increments of Δy = 60 km and Δz = 200 m. The data are extracted at t = 4 days, and all of the data in the tables are for the lowest level (z = 100 m).

Table 1 contains the frontal scale d for various combinations of the diffusion coefficients. The first column gives the values for zero vertical diffusion and the first row gives the values for zero horizontal diffusion. The smallest value of d occurs at the lowest level for each experiment except for the two with footnotes. In the two exceptional cases, the minimum occurs at the second point and this is caused by the vertical

diffusion of momentum. It may be seen that the value of d for each experiment is a little less than the sum of the values obtained from the experiments where one of the coefficients is zero.

Table 2 contains the frontal locations y_f for various combinations of the diffusion coefficients. In the first column, which is for zero vertical diffusion, the tilt decreases slightly with increasing horizontal diffusion coefficient. The combined experiments all show values which are closer to the A = 0 than to the $C_m = C_\theta = 0$ solutions. However, for each combination of C_m and C_θ, the tilt does decrease as A is increased. We conclude that the frontal scale is determined by both diffusion processes, but that the frontal tilt is determined principally by the vertical diffusion.

7. Conclusions

The numerical model of Williams (1972) is modified in this study to include horizontal and vertical diffusions of momentum and heat. The turbulent diffusions are represented with constant coefficients. An Ekman layer is added to the basic deformation field and some other terms which are related to the modified deformation field. The numerical solutions become quasi-steady within 1 - 2 days. These results suggest that atmospheric fronts form in a fairly short period of time (1 - 2 days) and then move in a state of quasi-balance where the frontogenetic processes are balanced by diffusion processes. The time scale of this second phase would be related to the time scale of the deformation field which caused the frontogenesis.

The solutions with only horizontal diffusion are similar to the transient solutions obtained in W72 at particular times. The horizontal scale at the lowest level follows approximately an $A^{1/2}$ dependence. The values obtained are less than the exact quasi-geostrophic solutions at z = 0 and they approach the latter as A increases. For reasonable values of A the scale is close to the quasi-geostrophic value, but the structure is very different since the quasi-geostrophic solutions contain no vertical tilt.

The solutions with only vertical diffusion are strongly dependent on the ratio of C_m to C_θ. All of these solutions show a deeper region

of large gradient than for the solutions with only horizontal diffusion. When C_θ is held fixed, the scale d shows little change as C_m is increased. On the other hand, when C_m is held fixed, d increases rapidly with increasing C_θ. The frontal tilt increases when C_m is held fixed and C_θ is decreased. The solutions for $C_m = 0$ or $C_\theta = 0$ are not acceptable steady solutions.

The solutions which include both horizontal and vertical diffusion are combinations of the separate solutions. The values for d are a little less than the sum of the values from each of the diffusion processes. The tilt of the fronts is principally determined by the vertical diffusion effects.

The steady-state frontal solutions obtained in this paper are reasonable with respect to observed fronts. The vertical diffusion terms are clearely required to give the proper structure near the surface. Both C_m and C_θ must be included although a value C_θ that is somewhat less than C_m may be appropriate. The importance of the horizontal diffusion processes can probably be determined only from turbulence studies in frontal zones.

The solutions found in this paper would be affected if nonlinear diffusion coefficients were used, but we expect the same general type of solution. However, if C_m were allowed to decrease above the friction layer, the maximum gradient might occur higher in the atmosphere.

The tilt of the solutions obtained would be modified if the whole system were allowed to have a net translation. Then it would be possible to distinguish between cold and warm fronts. The addition of latent heat should be important in determining the structure of many fronts.

Acknowledgements

The author wishes to thank Prof. G. J. Haltiner for reading the manuscript and for making several useful comments on it. The manuscript was carefully typed by Miss B. Dunbar and the figures were drafted by Mr. M. McDermet. This research was supported by the Environmental Prediction Research Facility and the Foundation Research Program at the Naval Postgraduate School which is funded by the Chief of Naval Research. The numerical computations were performed by the W. R. Church Computer Center.

REFERENCES

Deardorff, J. W., 1970: A three-dimensional numerical investigation of the idealized planetary boundary layer. Geophysical Fluid Dynamics, I, 377-410.

_____, 1972: Parameterization of the planetary boundary layer for use in general circulation models. Mon. Wea. Rev., 100, 93-106.

Estoque, M. A., 1960: Convective heat flux near the earth's surface. Cumulus Dynamics. New York, Pergamon Press, 39-43.

Hoskins, B. J., 1971: Atmospheric fronogenesis models: Some solutions. Quart. J. Roy. Meteor. Soc., 97, 139-153.

_____, 1972: Non-Boussinesq effects and further development in a model of upper tropospheric fronogenesis. Quart. J. Roy. Meteor. Soc., 98, 532-541.

_____, and F. P. Bretherton, 1972: Atmospheric frontogenesis models: Mathematical formulation and solution. J. Atmos. Sci, 29, 11-37.

Leith, C. E., 1968: Diffusion approximations for two-dimensional turbulence, Phys. Fluids, 11, 671-674.

Mak, M.-K.,1972: Steady, neutral planetary boundary layer forced by a horizontally non-uniform flow. J. Atmos. Sci., 29, 707-717.

Smagorinsky, J., 1963: General circulation experiments with the primitive equations. Mon. Wea. Rev., 91, 99-165.

Welander, P., 1963: Steady plane fronts in a rotating fluid. Tellus, 15, 33-43.

Williams, R. T., 1967: Atmospheric frontogenesis: A numerical experiment. J. Atmos. Sci., 24, 627-641.

_____, 1972: Quasi-geostrophic versus non-geostrophic frontogenesis. J. Atmos. Sci, 29, 3-10.

Table 1. Values of d in kilometers

C_m, C_θ / A	0,0	10, 1.25	10, 10	1.25, 5
0	-----	172	399	241
3×10^4	94	239	450	291
10^5	181	321	523	370
5×10^5	492	666[1]	828[2]	644

1 Minimum at z = 300 m of 631.

2 Minimum at z = 300 m of 827.

Table 2. Values of y_f in kilometers

C_m, C_θ / A	0,0	10, 1.25	10, 10	1.25, 5
0	----	-1010	-820	-720
3×10^4	-545	-995	-805	-715
10^5	-540	-985	-755	-700
5×10^5	-510	-985	-715	-640

FIGURE CAPTIONS

Figure 1. Time variation of the frontal scale at z = 167 m for experiments with only horizontal diffusion.

Figure 2. Cross sections of $\theta' = \theta - \overline{\theta}_I$ for A = 5 x 10^5 $m^2 sec^{-1}$ and A = 3 x 10^4 $m^2 sec^{-1}$ at t = 4 days.

Figure 3. Cross section of u for A = 5 x 10^5 $m^2 sec^{-1}$ and A = 3 x 10^4 $m^2 sec^{-1}$ at t = 3 days.

Figure 4. The variation of the frontal scale at z = 167 m as a function of the horizontal diffusion coefficient.

Figure 5. Time variation of the frontal scale at z = 100 m for experiments with only vertical diffusion.

Figure 6. Cross section of θ' for 3 combinations of C_m and C_θ at t = 4 days.

Figure 7. Cross sections of u for 3 combinations of C_m and C_θ at t = 4 days.

Figure 8. The frontal scale and frontal location as functions of C_m and C_θ. These data are for z = 100 m and t = 4 days.

Fig. 1

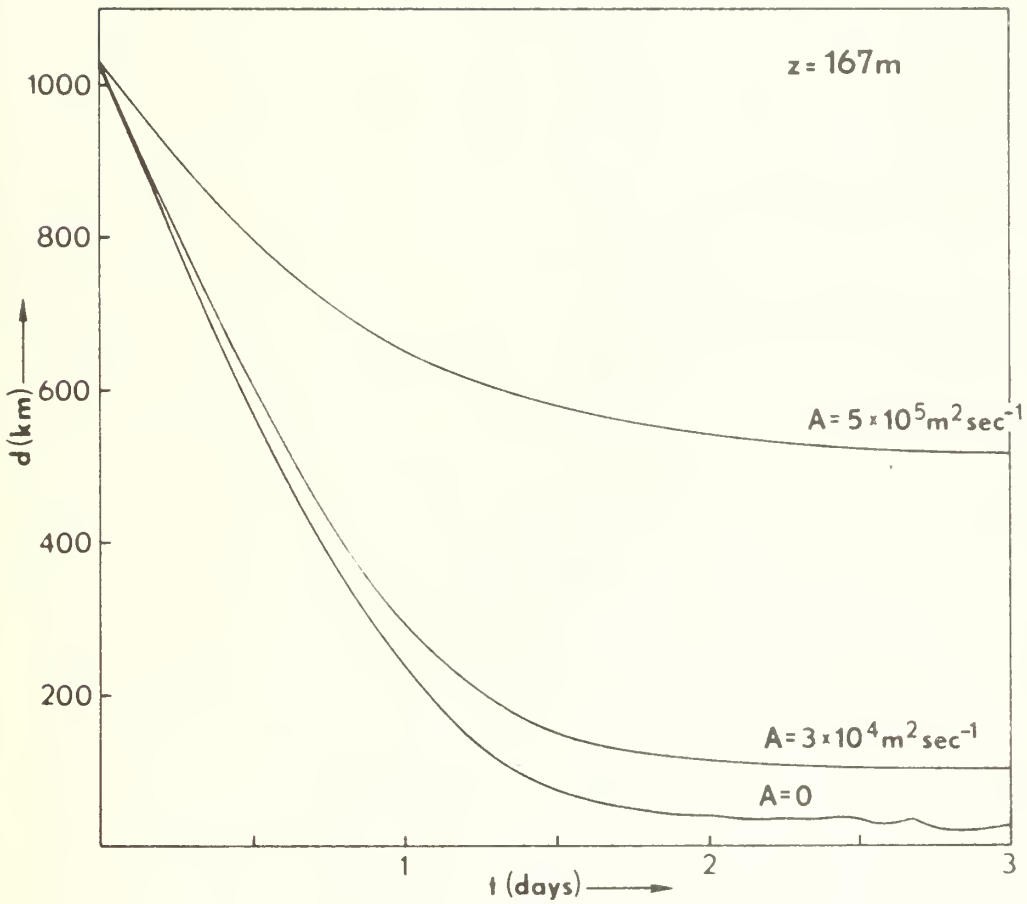
z = 167m
1000
800
600
400
200
d (km)
A = 5 x 10^5 m^2 sec^-1
A = 3 x 10^4 m^2 sec^-1
A = 0
1
2
3
t (days)

Fig. 2

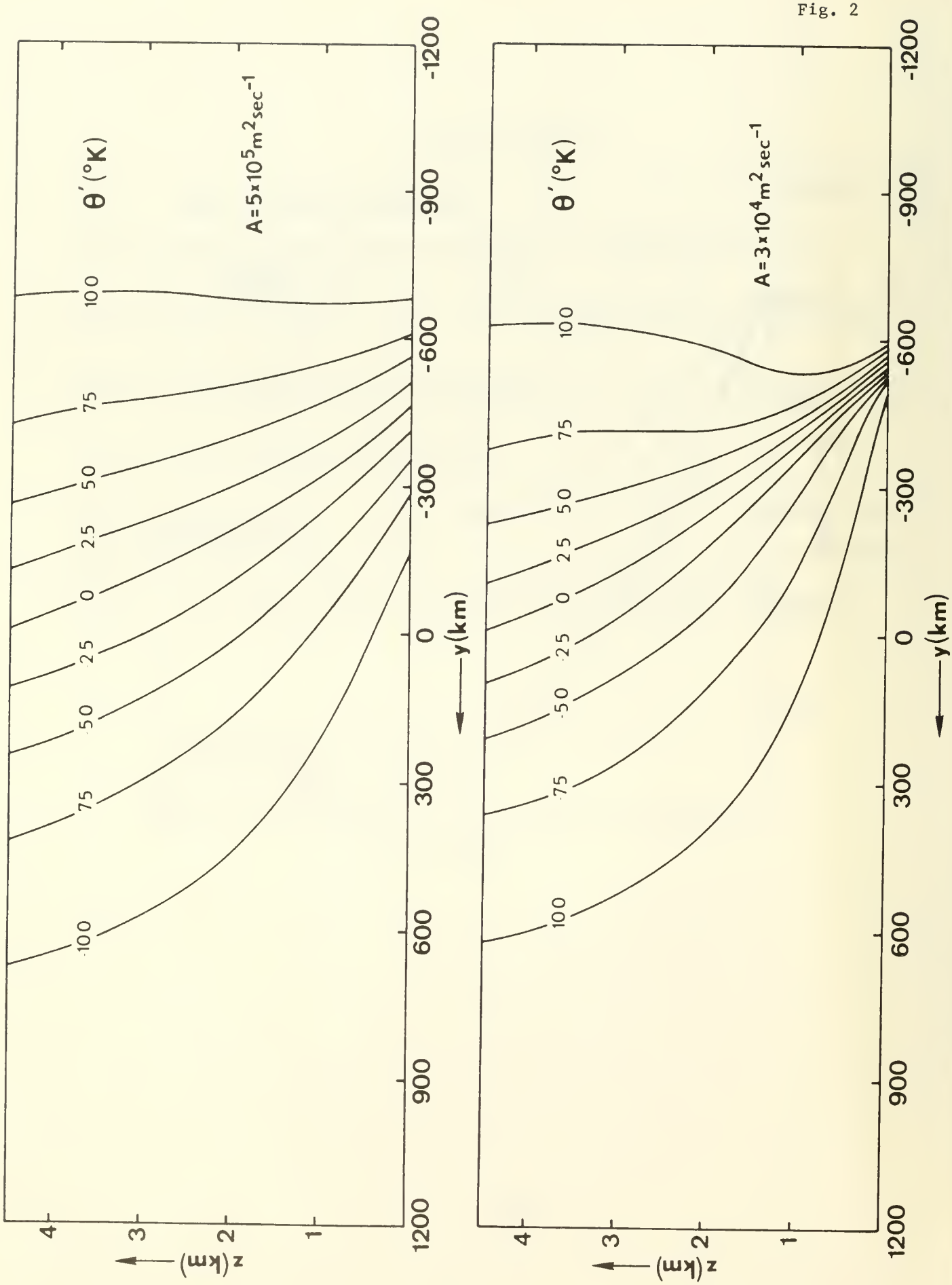
θ′(°K)
A=5×10⁵m²sec⁻¹
100
75
50
25
0
25
50
75
100
-1200
-900
-600
-300
0
300
600
900
1200
y(km)
z(km)
1
2
3
4
θ′(°K)
A=3×10⁴m²sec⁻¹
100
75
50
25
0
25
50
75
100
-1200
-900
-600
-300
0
300
600
900
1200
y(km)
z(km)
1
2
3
4

Fig. 3

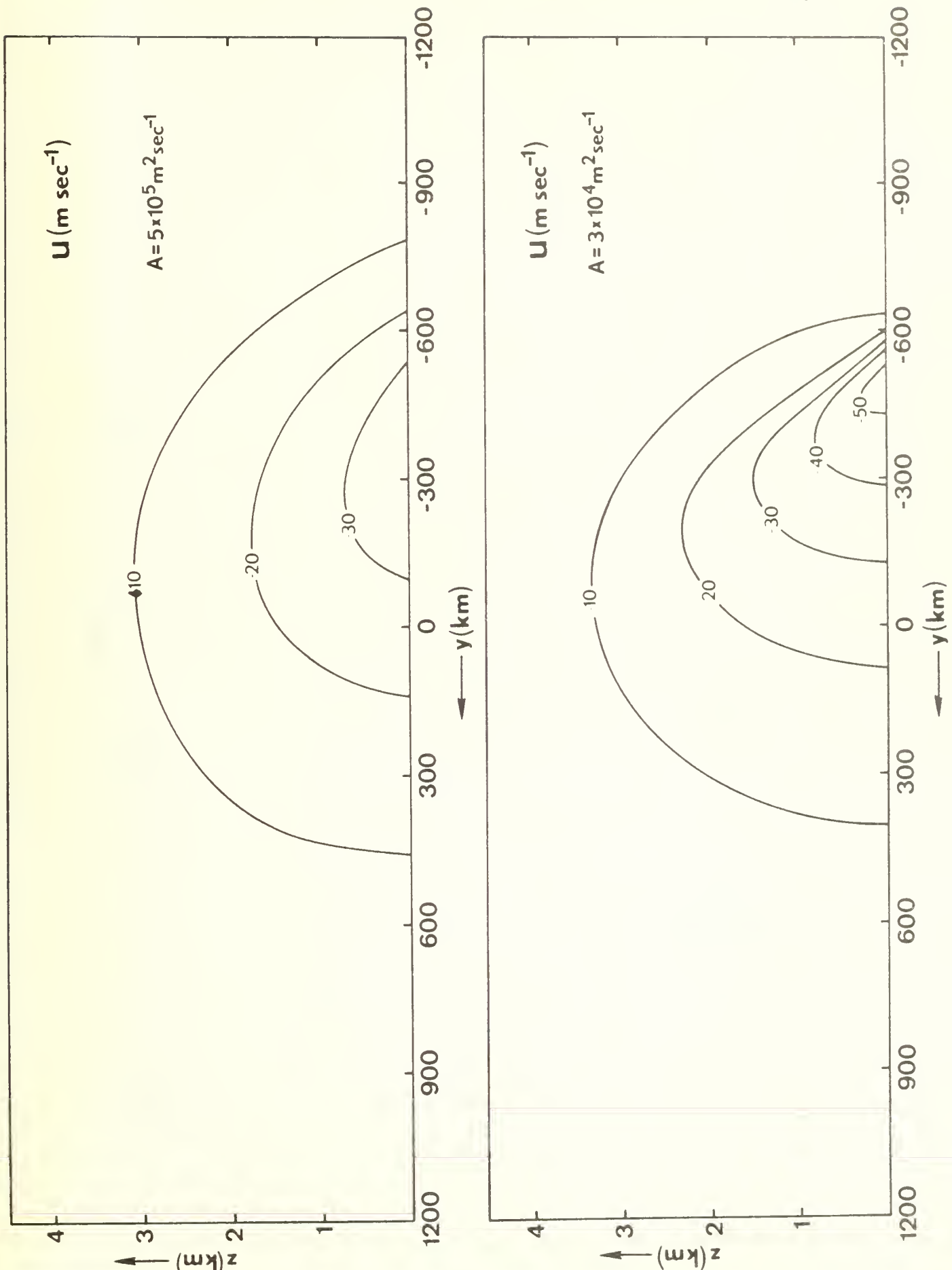
U (m sec^{-1})
A = 5×10^5 m^2 sec^{-1}
10
20
30
z (km)
y (km)
-1200
-900
-600
-300
0
300
600
900
1200
1
2
3
4
U (m sec^{-1})
A = 3×10^4 m^2 sec^{-1}
10
20
30
40
50
z (km)
y (km)

Fig. 4

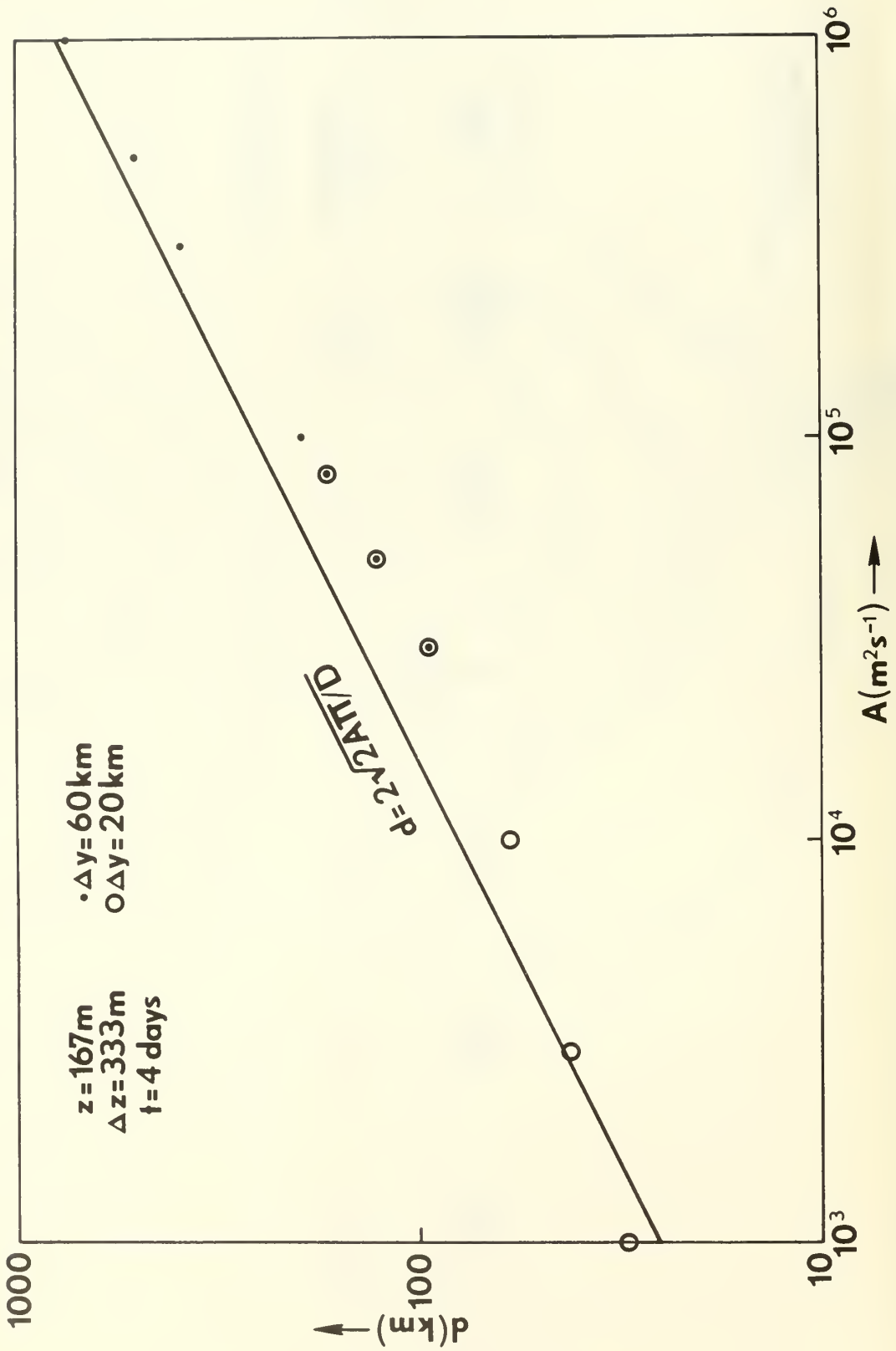
1000
100
10
d(km)
10^3
10^4
10^5
10^6
A(m^2s^{-1})
$d=2\sqrt{2ATt/D}$
z=167m
Δz=333m
t=4 days
•Δy=60km
○Δy=20km

Fig. 5

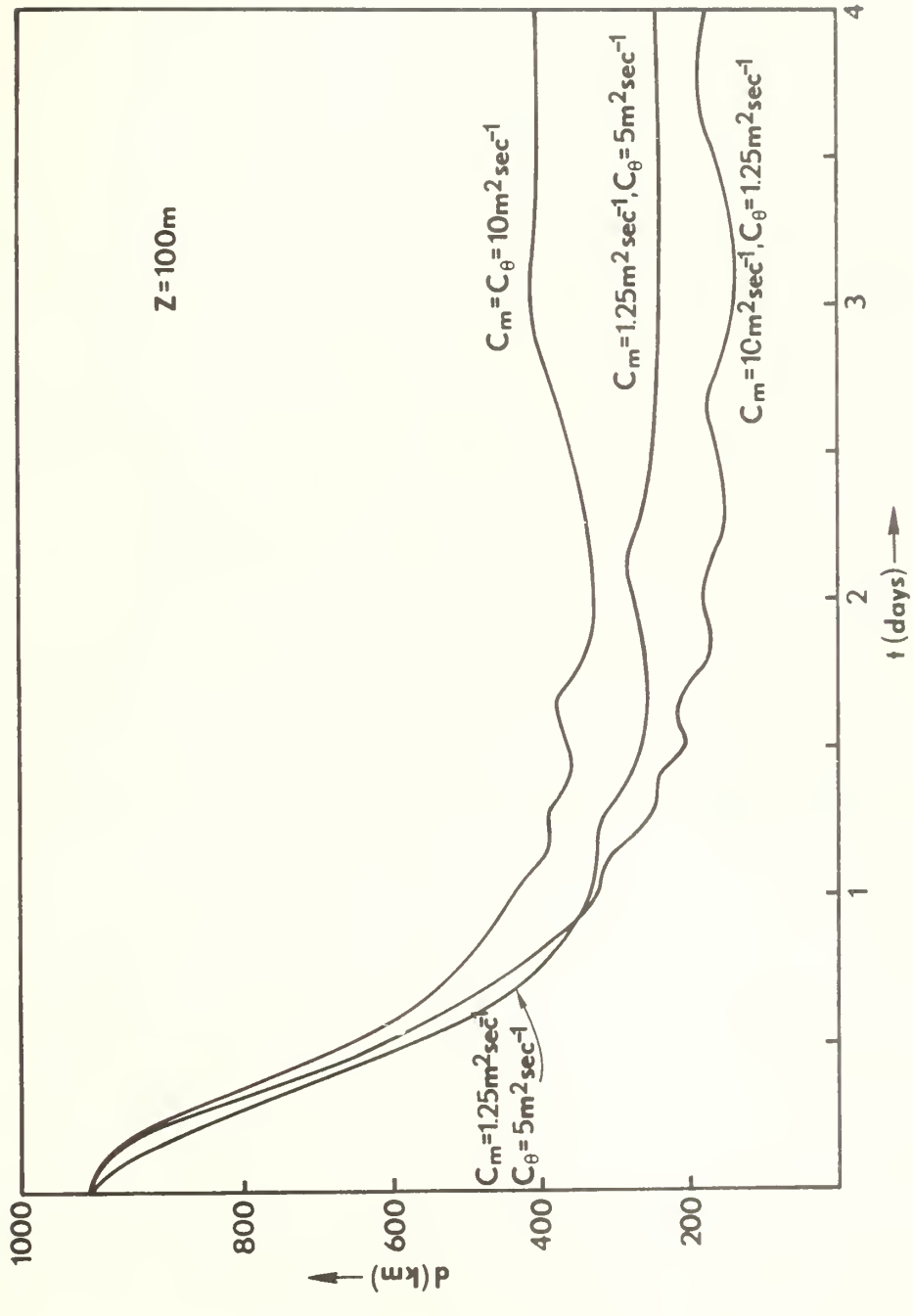
Z=100m
$C_m = C_\theta = 10 m^2 sec^{-1}$
$C_m = 1.25 m^2 sec^{-1}, C_\theta = 5 m^2 sec^{-1}$
$C_m = 10 m^2 sec^{-1}, C_\theta = 1.25 m^2 sec^{-1}$
$C_m = 1.25 m^2 sec^{-1}$
$C_\theta = 5 m^2 sec^{-1}$
d(KE)
t (days)
1000
800
600
400
200
1
2
3
4

Fig. 6

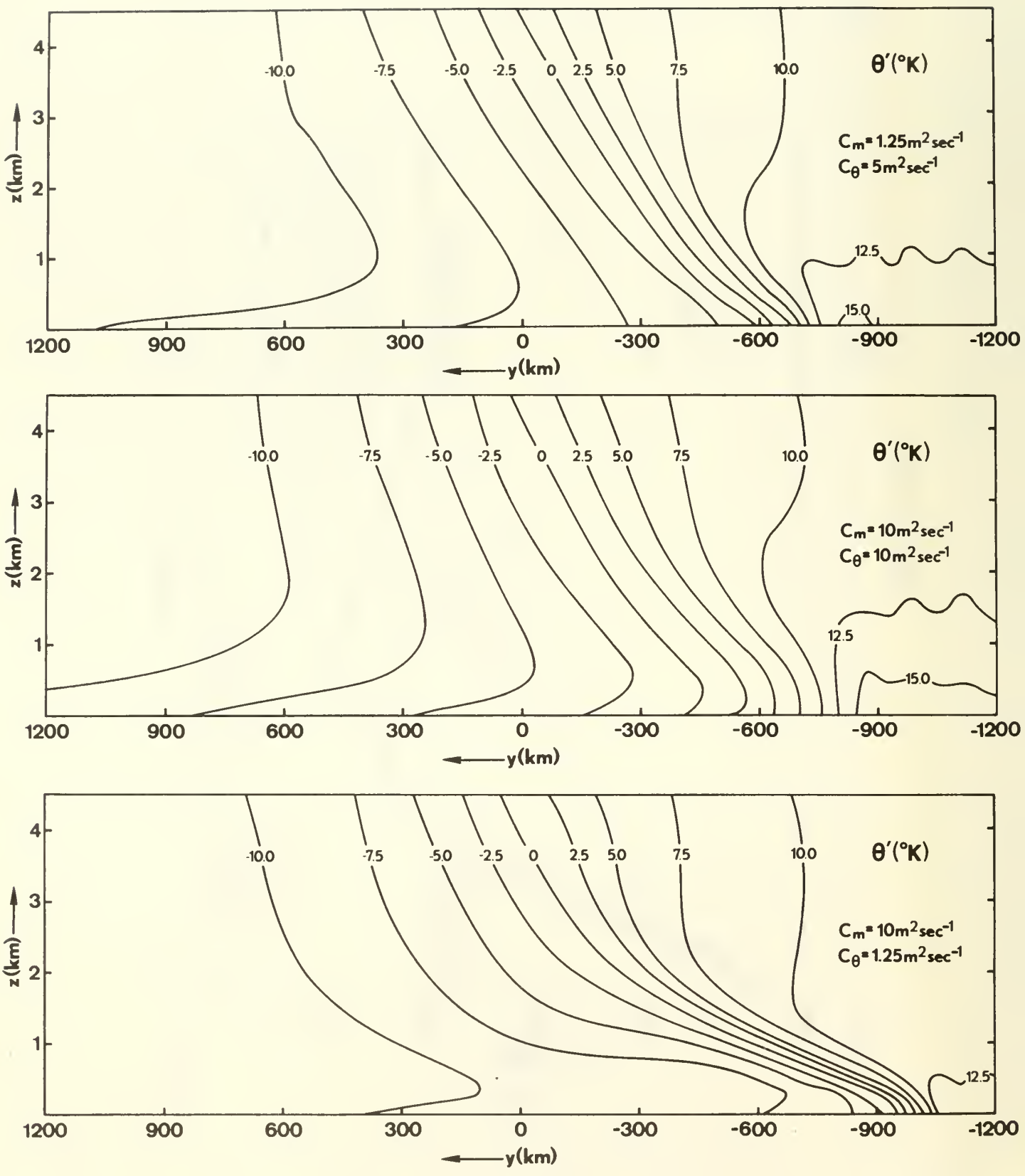
θ'(°K)
-10.0
-7.5
-5.0
-2.5
0
2.5
5.0
7.5
10.0
12.5
15.0
$C_m = 1.25 m^2 sec^{-1}$
$C_\theta = 5 m^2 sec^{-1}$
z(km)
y(km)
1200
900
600
300
0
-300
-600
-900
-1200
θ'(°K)
$C_m = 10 m^2 sec^{-1}$
$C_\theta = 10 m^2 sec^{-1}$
θ'(°K)
$C_m = 10 m^2 sec^{-1}$
$C_\theta = 1.25 m^2 sec^{-1}$

Fig. 7

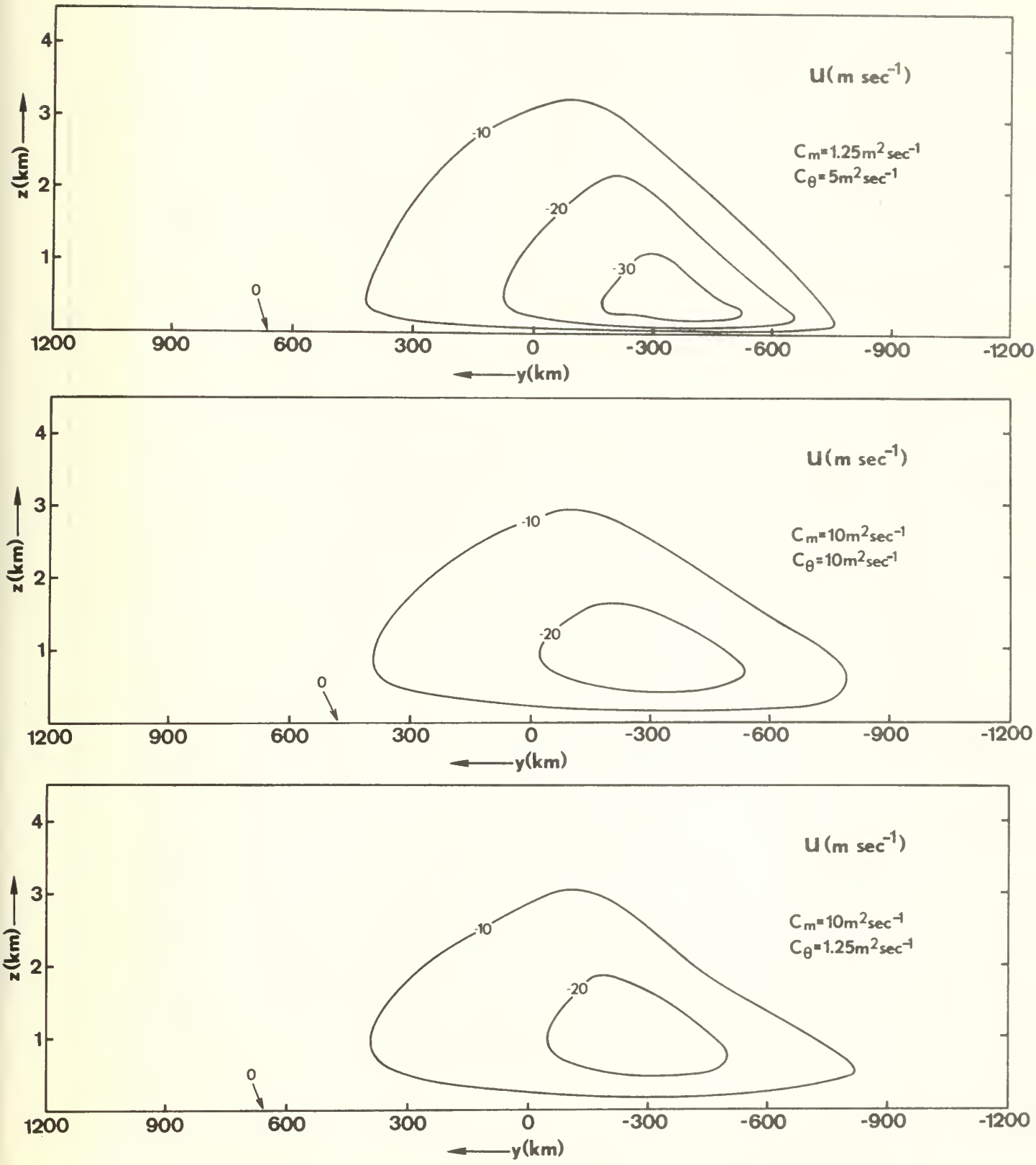
U(m sec^{-1})
C_m=1.25m^{2}sec^{-1}
C_θ=5m^{2}sec^{-1}
-10
-20
-30
0
z(km)
y(km)
4
3
2
1
1200
900
600
300
0
-300
-600
-900
-1200
U(m sec^{-1})
C_m=10m^{2}sec^{-1}
C_θ=10m^{2}sec^{-1}
-10
-20
0
z(km)
y(km)
U(m sec^{-1})
C_m=10m^{2}sec^{-1}
C_θ=1.25m^{2}sec^{-1}
-10
-20
0
z(km)
y(km)

Fig. 8

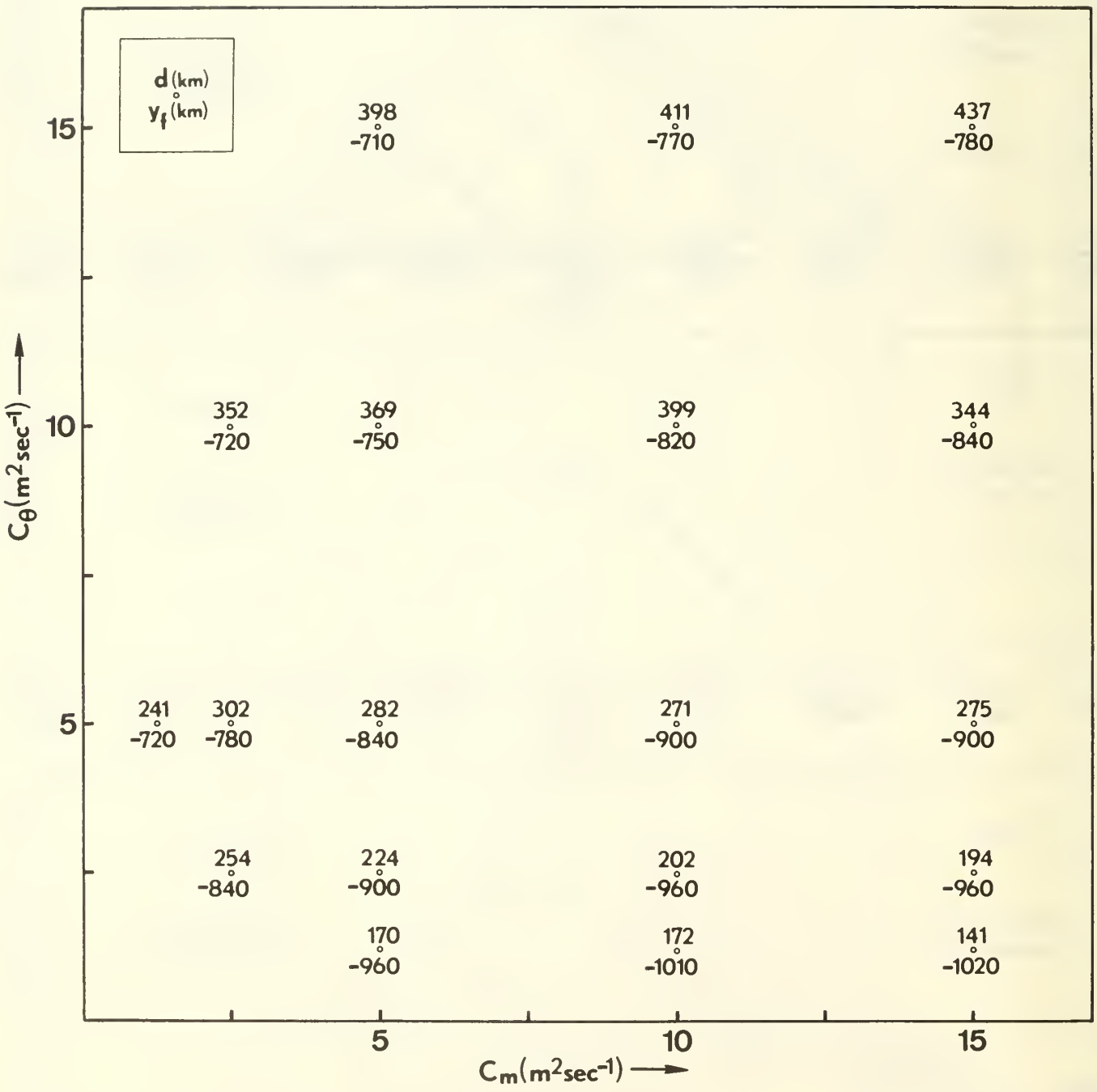
d (km)
y_f (km)
398
-710
411
-770
437
-780
352
-720
369
-750
399
-820
344
-840
241
-720
302
-780
282
-840
271
-900
275
-900
254
-840
224
-900
202
-960
194
-960
170
-960
172
-1010
141
-1020
15
10
5
5
10
15
$C_\theta (m^2 sec^{-1})$
$C_m (m^2 sec^{-1})$

DISTRIBUTION LIST

Defense Documentation Center Cameron Station Alexandria, Virginia 22314	12
Library, Code 0212 Naval Postgraduate School Monterey, California 93940	2
Dr. R. T. Williams, Code 51Wu Department of Meteorology Naval Postgraduate School Monterey, California 93940	20
Commanding Officer Naval Weather Service Command 3101 Building 200 Washington Navy Yard Washington, D. C. 20390	1
Officer in Charge Environmental Prediction Research Facility Naval Postgraduate School Monterey, California 93940	10
Dean of Research Naval Postgraduate School Monterey, California 93940	2
Commanding Officer Fleet Numerical Weather Central Naval Postgraduate School Monterey, California 93940	4
AFCRL - Research Library L. G. Hanscom Field Attn: Nancy Davis/Stop 29 Bedford, Massachusetts 01730	1
Director, Naval Research Laboratory Attn: Tech. Services Information Officer Washington, D. C. 20390	1
Department of Meteorology Code 51 Naval Postgraduate School Monterey, California 93940	1

Department of Oceanography 1
Code 58
Naval Postgraduate School
Monterey, California 93940

Office of Naval Research 1
Department of the Navy
Washington, D. C. 20360

Commander, Air Weather Service 1
Military Airlift Command
United States Air Force
Scott Air Force Base, Illinois 62226

Dr. F. J. Winninghoff 1
1085 Steeles Avenue, #503
Willowdale (Toronto), Ontario
M2R2T1

Professor J. Bjerknes 1
Department of Meteorology
UCLA
Los Angeles, California 90024

Atmospheric Sciences Library 1
National Oceanic and Atmospheric Administration
Silver Spring, Maryland 20910

Professor Victor Starr 1
Department of Meteorology
M.I.T.
Cambridge, Massachusetts 03139

Dr. J. Pedlosky 1
Department of Geophysical Sciences
University of Chicago
Chicago, Illinois 60637

Dr. Joanne Simpson 1
Experimental Meteorology Branch
National Oceanic and Atmospheric Administration
Coral Gables, Florida 33124

Dr. G. C. Asnani 1
Observatory
Poona 5, India

National Center for Atmospheric Research 1
Box 1470
Boulder, Colorado 80302

Dr. Fred Shuman, Director 1
National Meteorological Center
National Oceanic and Atmospheric Administration
Suitland, Maryland 20390

Dr. J. Smagorinsky, Director 1
Geophysical Fluid Dynamics Laboratory
Princeton University
Princeton, New Jersey 08540

Professor N. A. Phillips 1
Department of Meteorology
M. I. T.
Cambridge, Massachusetts 02139

Dr. B. J. Hoskins 1
Geophysical Fluid Dynamics Program
Princeton University
Princeton, New Jersey 08540

Professor J. Holmboe 1
Department of Meteorology
UCLA
Los Angeles, California 90024

Professor J. G. Charney 1
54-1424
M. I. T.
Cambridge, Massachusetts 02139

Dr. F. Sanders 1
Department of Meteorology
M.I.T.
Cambridge, Massachusetts 02139

Professor K. Ooyama 1
National Center for Atmospheric Research
P.O. Box 1470
Boulder, Colorado 80302

Dr. M. G. Wurtele 1
Department of Meteorology
UCLA
Los Angeles, California 90024

Dr. A. Arakawa 1
Department of Meteorology
UCLA
Los Angeles, California 90024

Dr. G. Haltiner, Chairman 1
Department of Meteorology, Code 51Ha
Naval Postgraduate School
Monterey, California 93940

Dr. R. L. Haney 1
Department of Meteorology, Code 51Hy
Naval Postgraduate School
Monterey, California 93940

Dr. R. Elsberry 1
Department of Meteorology, Code 51Es
Naval Postgraduate School
Monterey, California 93940

Dr. C. P. Chang 1
Department of Meteorology, Code 51Cj
Naval Postgraduate School
Monterey, California 93940

Dr. R. Renard 1
Department of Meteorology, Code 51Rd
Naval Postgraduate School
Monterey, California 93940

Dr. J. Galt 1
Department of Oceanography, Code 58
Naval Postgraduate School
Monterey, California 93940

Dr. K. Davidson ~~1~~
Department of Meteorology, Code 51Ds
Naval Postgraduate School
Monterey, California 93940

Dr. R. Alberty 1
National Severe Storms Laboratory
1313 Halley Circle
Norman, Oklahoma 73069

Professor Peter J. Gierasch 1
Space Sciences Building
Cornell University
Ithaca, New York 14850

Dr. Peter H. Stone 1
Institute for Space Studies
2880 Broadway
New York, New York 10025

Dr. S. Piacsek
Code 7750
Naval Research Laboratory
Washington, D. C. 20390 — 1

Dr. E. N. Lorenz
Department of Meteorology
M. I. T.
Cambridge, Massachusetts 02139 — 1

Dr. D. Houghton
Department of Meteorology
University of Wisconsin
Madison, Wisconsin 53706 — 1

Dr. S. K. Kao
Department of Meteorology
University of Utah
Salt Lake City, Utah 84112 — 1

Dr. A. P. Ingersoll
Division of Geological and Planetary Sciences
California Institute of Technology
Pasadena, California 91101 — 1

Dr. J. Wallace
Department of Atmospheric Sciences
University of Washington
Seattle, Washington 98105 — 1

Dr. J. Holton
Department of Atmospheric Sciences
University of Washington
Seattle, Washington 98105 — 1

Dr. J. Young
Department of Meteorology
University of Wisconsin
Madison, Wisconsin 53706 — 1

Dr. T. Ogura
Laboratory for Atmospheric Research
University of Illinois
Urbana, Illinois 61801 — 1

Dr. Y. Sasaki
Department of Meteorology
University of Oklahoma
Norman, Oklahoma 73069 — 1

Dr. J. Mahlman 1
Geophysical Fluid Dynamics Laboratory
Princeton University
Princeton, New Jersey 08540

Dr. R. Alexander 1
The Rand Corporation
1700 Main Street
Santa Monica, California 90406

Dr. J. L. Lewis 1
Laboratory for Atmospheric Research
University of Illinois
Urbana, Illinois 61801

Dr. S. Mudrick 1
AFCRL (LYD)
L. G. Hanscom Field
Bedford, Massachusetts 01730

Dr. W. L. Gates 1
The Rand Corporation
1700 Main Street
Santa Monica, California 90406

Professor F. Bretherton 1
John Hopkins University
Baltimore, Maryland 21218

UNCLASSIFIED

SECURITY CLASSIFICATION OF THIS PAGE (*When Date Entered*)

REPORT DOCUMENTATION PAGE

READ INSTRUCTIONS BEFORE COMPLETING FORM

1. REPORT NUMBER: NPS-51Wu 73081A	2. GOVT ACCESSION NO.
3. RECIPIENT'S CATALOG NUMBER	
4. TITLE (*and Subtitle*): Numerical Simulation of Steady-State Fronts	5. TYPE OF REPORT & PERIOD COVERED: Annual Report 1 July 1972-30 June 1973
6. PERFORMING ORG. REPORT NUMBER: NPS-51Wu 73081A	
7. AUTHOR(*s*): Roger T. Williams	8. CONTRACT OR GRANT NUMBER(*s*): P.O. No.2-0013 EPRF
9. PERFORMING ORGANIZATION NAME AND ADDRESS: Naval Postgraduate School, Monterey, CA 93940	10. PROGRAM ELEMENT, PROJECT, TASK AREA & WORK UNIT NUMBERS
11. CONTROLLING OFFICE NAME AND ADDRESS: Chief of Naval Research, Arlington, VA ; Environmental Prediction Research Facility, Monterey CA	12. REPORT DATE: August 1973 13. NUMBER OF PAGES: 33
14. MONITORING AGENCY NAME & ADDRESS(*if different from Controlling Office*): Naval Postgraduate School, Monterey, CA 93940	15. SECURITY CLASS. (*of this report*): UNCLASSIFIED 15a. DECLASSIFICATION/DOWNGRADING SCHEDULE

16. DISTRIBUTION STATEMENT (*of this Report*)

Approved for public release; distribution unlimited.

17. DISTRIBUTION STATEMENT (*of the abstract entered in Block 20, if different from Report*)

18. SUPPLEMENTARY NOTES

19. KEY WORDS (*Continue on reverse side if necessary and identify by block number*)

Fronts

Friction

Numerical Integration

20. ABSTRACT (*Continue on reverse side if necessary and identify by block number*)

The numerical frontogenesis model of Williams (1972) is modified to include horizontal and vertical turbulent diffusions of heat and momentum. The turbulent diffusions are represented with constant coefficients, and an Ekman layer is added to the basic deformation field. The numerical solutions show realistic quasi-steady fronts forming within 1 - 2 days. These solutions are examined and compared over a wide range of the various coefficients.

DD FORM 1 JAN 73 1473 EDITION OF 1 NOV 65 IS OBSOLETE
S/N 0102-014-6601 |
(Page 1)

UNCLASSIFIED

SECURITY CLASSIFICATION OF THIS PAGE (*When Date Entered*)